

Coherence properties of entangled light beams generated by parametric down-conversion: Theory and experiment

Adel Joobeur

Department of Electrical and Computer Engineering, University of Wisconsin, Madison, Wisconsin 53706

Bahaa E. A. Saleh

Department of Electrical and Computer Engineering, Boston University, Boston, Massachusetts 02215

Todd S. Larchuk

Department of Electrical Engineering, Columbia University, New York, New York 10027

Malvin C. Teich

Department of Electrical and Computer Engineering, Boston, Massachusetts 02215

(Received 1 May 1995)

Using a multidimensional Gaussian approximation of the wave function for the signal and idler light generated by spontaneous parametric down-conversion, we derive analytical expressions for the second-order coherence function and the fourth-order coherence function (which is proportional to the signal-idler photon coincidence rate). The magnitudes of these functions are expressed as products of Gaussian functions of the azimuthal angles, the polar angles, and the time delay. Their widths determine six parameters: the coherence angles and coherence time, and the entanglement angles and entanglement time. We show how these parameters are governed by the pump-beam waist, the pump spectral width, and the crystal length. We thereby derive relations analogous to the van Cittert–Zernike theorem and the Siegert relation for thermal light. We show that the normalized photon coincidence rate decreases sharply as the signal and idler apertures become mismatched or misaligned. We experimentally confirm this latter prediction by using parametrically down-converted light obtained from a LiIO_3 crystal pumped by Kr^+ -ion laser radiation at 413 nm.

PACS number(s): 42.50.Ar, 42.50.Dv, 42.65.Ky

I. INTRODUCTION

Spontaneous parametric down-converted light has unusual spatiotemporal coherence properties that are imposed by the requirements of energy and phase matching [1–7]. The signal and idler beams have spectra that vary with direction, forming rainbow-type rings, and the coherence angle and coherence time are also dependent on direction [1,4,7,8], so that these beams are clearly not cross-spectrally pure in second order [9]. The fourth-order coherence function determines the coincidence rate of the signal and idler photons as a function of their time delay and propagation directions and therefore governs the degree of spatiotemporal entanglement between the twin photons [2–7,10–14]. The entanglement angles and the entanglement time, representing angular and temporal widths of the fourth-order coherence function, are also dependent on direction [3,7]. When apertures are used to collect signal and idler photons, the ratios between the aperture angles and the corresponding entanglement angles have a significant effect on the rate of photon coincidence. Any misalignment of either of the apertures with respect to the direction of maximum entanglement also has a strong effect on the measured coincidence rates [7].

In the ideal case of a monochromatic, plane-wave pump interacting with an infinite-length nonlinear crystal, energy and momentum conservation restrict the down-converted light so that it is monochromatic in each direction, and each signal direction has one and only one matching idler direction. Thus the entanglement angle is zero everywhere and the coincidence rate at matched directions is independent of the

time delay, i.e., the entanglement time is infinite.

For a crystal of finite length, however, momentum mismatching in the longitudinal direction is tolerated. For a pump of finite spectral width, this also applies and, in addition, energy matching is more flexible. As a result, the signal in any given direction is no longer monochromatic and is entangled with the idler photons within a sector of finite angle in the polar direction, viz., the polar entanglement angle [7]. For a plane-wave pump, the entanglement angle in the azimuthal direction is zero and the entanglement time remains infinite [3,7]. When the pump beam has a finite transverse width, however, the pump wave vector occupies a cone of finite angle so that momentum conservation in the transverse direction can be satisfied in more than one way. This too affects both the coherence and entanglement angles and results in a nonvanishing azimuthal entanglement angle, as well as a finite entanglement time. All of these effects are, of course, present in real experiments.

In a previous study [7] we developed a theory for the second- and fourth-order spatiotemporal coherence properties of spontaneous parametrically down-converted light, assuming a crystal of finite length and a pump of finite spectral width. However, the pump was assumed to be a plane wave. In this paper we extend our theory to include the effect of the pump transverse width and develop the theory further to study the interplay among these three effects in determining the coherence and entanglement angles and times. We also report the results of an experiment in which the signal-idler photon coincidence rate was observed through apertures of various sizes and different misalignments from the optimal

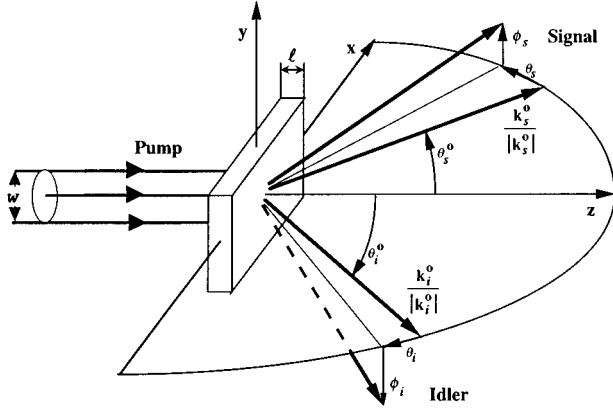


FIG. 1. Geometry for spontaneous parametric down-conversion arrangement. Arrow directions indicate positive-sign conventions for signal and idler polar (θ) and azimuthal (ϕ) angles.

directions. The experimental results agree with the theory.

II. QUANTUM STATE OF DOWN-CONVERTED LIGHT

Consider type-I (ooe) parametric down-conversion in a crystal of length l , with ordinary and extraordinary refractive indices $n_o(\omega)$ and $n_e(\omega)$ at the angular frequency ω and an effective second-order nonlinear susceptibility $\chi_{\text{eff}}^{(2)}$. The pump is a beam pointing in the \hat{z} direction, as depicted in Fig. 1, with a waist w in the transverse direction and a spectral width $\Delta\omega_p$. The pump field is treated classically and is expressed by the spectral expansion

$$\mathbf{E}(\mathbf{r};t) = \hat{\mathbf{e}} f(x,y) \int_0^\infty d\omega_p A(\omega_p) \exp\left[i\left(\frac{\omega_p n_e(\omega_p)}{c} z - \omega_p t\right)\right] + \text{c.c.}, \quad (1)$$

where $\hat{\mathbf{e}}$ is the pump extraordinary polarization direction and $f(x,y)$ is the pump amplitude distribution in the transverse plane, which is assumed to be the same throughout the crystal and to have a width w . The pump spectral width $\Delta\omega_p$, determined from $A(\omega_p)$, is assumed to be sufficiently small so that the beam's spatial distribution in the transverse plane is frequency independent. Here c is the speed of light in free space.

Using this expression for the pump field, in first-order perturbation with the quadratic interaction Hamiltonian, the state of the down-converted light can be shown to be a superposition of the vacuum state and a state with a single photon in each of the signal and idler beams. This twin state, expressed as an expansion in the wave-vector space [7,15], is

$$|\mathcal{T}\rangle = \iint d\mathbf{k}_s d\mathbf{k}_i \psi(\mathbf{k}_s, \mathbf{k}_i) |\mathbf{k}_s\rangle_s |\mathbf{k}_i\rangle_i, \quad (2a)$$

where \mathcal{T} denotes the twin state,

$$\begin{aligned} \psi(\mathbf{k}_s, \mathbf{k}_i) &= \chi_{\text{eff}}^{(2)} A(\omega_s + \omega_i) F(\mathbf{k}_{s\perp} + \mathbf{k}_{i\perp}) \\ &\times l \operatorname{sinc}\left[\frac{l}{2\pi}\{k_{z,s} + k_{z,i} - k_p(\omega_s + \omega_i)\}\right] \end{aligned} \quad (2b)$$

is the wave function in \mathbf{k} space, $\operatorname{sinc}(x) \equiv \sin(\pi x)/\pi x$, and $F(\mathbf{k}_\perp)$ denotes the two dimensional Fourier transform of $f(x,y)$. The wave vectors \mathbf{k}_p , \mathbf{k}_s , and \mathbf{k}_i of the pump, the signal, and the idler have magnitudes $\omega_p n_e(\omega_p)/c$, $\omega_s n_o(\omega_s)/c$, and $\omega_i n_o(\omega_i)/c$, respectively. The wave function in Eq. (2b) is the same as its counterpart in [7] [see Eq. (6) in [7]], except for the delta function $\delta(\mathbf{k}_\perp)$, which is replaced here by $F(\mathbf{k}_\perp)$, accounting for the finiteness of the pump beam waist.

It is convenient to select central signal and idler wave vectors \mathbf{k}_s^0 and \mathbf{k}_i^0 that are phase and frequency matched to the central pump wave vector $\mathbf{k}_p^0 = k_p^0 \hat{z}$ and to take the wave vectors \mathbf{k}_s^0 and \mathbf{k}_i^0 to lie in the x - z plane. These central wave vectors are determined by their azimuthal angles $\phi_s^0 = 0$ and $\phi_i^0 = \pi$, polar angles θ_s^0 and θ_i^0 (internal to the crystal), and frequencies ω_s^0 and ω_i^0 , as shown in Fig. 1. We are only interested in directions $\hat{\mathbf{k}}_s$ and $\hat{\mathbf{k}}_i$ and in frequencies ω_s and ω_i in the vicinity of these central directions and frequencies. To obtain an explicit expression for the wave function in Eq.(2b), we expand the wave vectors \mathbf{k}_s and \mathbf{k}_i to first order in frequency and in angular deviations from their central values, to obtain

$$\begin{aligned} \Delta k_x(\omega_s, \theta_s, \omega_i, \theta_i) &\equiv k_{sx} + k_{ix} = \frac{N_s \sin\theta_s^0}{c} \Omega_s - \frac{N_i \sin\theta_i^0}{c} \Omega_i \\ &+ \frac{2\pi n_s \cos\theta_s^0}{\lambda_s^0} \theta_s - \frac{2\pi n_i \cos\theta_i^0}{\lambda_i^0} \theta_i, \end{aligned} \quad (3a)$$

$$\Delta k_y(\phi_s, \phi_i) \equiv k_{sy} + k_{iy} = \frac{2\pi n_s \sin\theta_s^0}{\lambda_s^0} (\phi_s - \phi_i), \quad (3b)$$

and

$$\begin{aligned} \Delta k_z(\omega_s, \theta_s, \omega_i, \theta_i) &\equiv k_{sz} + k_{iz} - k_p \\ &= \frac{N_s \cos\theta_s^0 - N_p}{c} \Omega_s + \frac{N_i \cos\theta_i^0 - N_p}{c} \Omega_i \\ &- \frac{2\pi n_s \sin\theta_s^0}{\lambda_s^0} (\theta_s + \theta_i), \end{aligned} \quad (3c)$$

where $\Omega_j = \omega_j - \omega_j^0$, θ_j and ϕ_j are internal to the crystal and measured from their respective central values θ_j^0 and ϕ_j^0 as shown in Fig. 1, $n_j = n_o(\omega_j^0)$, and N_p and N_j are group indices of refraction ($j = s, i$). These equations give the components of the wave-vector mismatch and include dispersion. We also used the relation $k_{sx}^0 = k_{ix}^0$ (i.e., $n_s \lambda_s^0 \sin\theta_s^0 = n_i \lambda_i^0 \sin\theta_i^0$) to obtain Eqs. (3b) and (3c).

Using Eq. (3), the twin state can be expressed in the form

$$\begin{aligned} |\mathcal{T}\rangle &= \int d\omega_s d\theta_s d\phi_s \\ &\times \int d\omega_i d\theta_i d\phi_i \psi(\omega_s, \theta_s, \phi_s, \omega_i, \theta_i, \phi_i) \\ &\times |\omega_s, \theta_s, \phi_s\rangle_s |\omega_i, \theta_i, \phi_i\rangle_i, \end{aligned} \quad (4a)$$

where

$$\psi(\omega_s, \theta_s, \phi_s, \omega_i, \theta_i, \phi_i) = NA(\omega_s + \omega_i) \times F(\Delta \mathbf{k}_\perp) \operatorname{sinc}\left(\frac{l}{2\pi} \Delta k_z\right). \quad (4b)$$

Here the second-order susceptibility and the Jacobian needed in transforming from dk^3 to $d\omega d\theta d\phi$ are assumed to be slowly varying in comparison with the remaining function and are included in the normalization constant N . Equation (4) is the counterpart of Eq. (10) in [7].

The wave function is therefore the product of three functions, representing the effects of the pump spectral width, the pump beam width, and the crystal length. The properties of the emitted light are therefore governed by the three normalized variables $\Delta\omega_p/\omega_p^0$, λ_p^0/w , and λ_p^0/l representing these three effects, respectively. The ultimate goal of this paper is to examine the effect of these three variables on the coherence and entanglement properties of the signal and idler light.

III. COHERENCE FUNCTIONS

A. General results

In this section, general expressions for the second-order (amplitude) and fourth-order (intensity) coherence functions for the signal and idler fields of the down-converted light are determined. As in [7], the far-field electric-field operators are written in terms of annihilation and creation operators satisfying appropriate commutation relations. The coherence functions are then determined by averaging the appropriate field operators using Eq. (4a) for the twin state and integrating over time t to obtain the stationary results. Since the analysis is a straightforward generalization of that carried out in [7] we only report the results here.

Because the projected signal and idler states are single-photon states, the second-order coherence function at a point within the signal field and at another within the idler field vanishes. The second-order coherence function at pairs of points within the signal field is given by

$$G_{ss}^{(1)}(\theta_s, \phi_s, \theta'_s, \phi'_s; \tau) = \int d\omega_s S_{ss}^{(1)}(\theta_s, \phi_s, \theta'_s, \phi'_s; \omega_s) \exp(i\omega_s \tau), \quad (5a)$$

where

$$S_{ss}^{(1)}(\theta_s, \phi_s, \theta'_s, \phi'_s; \omega_s) = \int d\omega_i d\theta_i d\phi_i \psi^*(\omega_s, \theta'_s, \phi'_s, \omega_i, \theta_i, \phi_i) \times \psi(\omega_s, \theta_s, \phi_s, \omega_i, \theta_i, \phi_i) \quad (5b)$$

is the signal cross-power spectral density. In our previous paper [7], the dependence of this cross-power spectral density on the signal angles is described by a δ function, i.e., the signal field is spatially incoherent. This is a direct consequence of the plane-wave pump assumption and implies that the product wave functions in Eq. (5b) do not overlap when

the two signal directions are not the same. In this paper, the assumption of finite pump-beam waist results in nonvanishing polar and azimuthal coherence angles for the down-converted light, as will be seen later.

The fourth-order coherence function within the signal (or the idler) beam vanishes, so that only random coincidences arise within the signal (or the idler) beam. This is a consequence of the fact that the twin state projects into a one-photon state in the signal subspace and a one-photon state in the idler subspace.

The coincidence rate for a signal photon and an idler photon is determined by the signal-idler fourth-order coherence function [16]. Using an analysis similar to that in [7], we obtain

$$G_{si}^{(2)}(\theta_s, \phi_s, \theta_i, \phi_i; \tau) = \int d\Omega S_{si}^{(2)}(\theta_s, \phi_s, \theta_i, \phi_i; \Omega) \exp(i\Omega \tau), \quad (6a)$$

where

$$S_{si}^{(2)}(\theta_s, \phi_s, \theta_i, \phi_i; \Omega) = \int d\omega_s \int d\omega_i \psi^*(\omega_s, \theta_s, \phi_s, \omega_i, \theta_i, \phi_i) \times \psi(\omega_s - \Omega, \theta_s, \phi_s, \omega_i + \Omega, \theta_i, \phi_i) \quad (6b)$$

represents the fourth-order cross-power spectral density. It is straightforward to verify that $S_{si}^{(2)}(-\Omega) = S_{si}^{(2)*}(\Omega)$, indicating that the fourth-order coherence function in Eq. (6a) is real. The integral in Eq. (6b) implies that, for fixed signal and idler directions, the overlap between $\psi^*(\omega_s, \omega_i)$ and $\psi(\omega'_s, \omega'_i)$ contributes to the cross-power spectral density at frequency Ω only if $\omega'_s = \omega_s - \Omega$ and $\omega'_i = \omega_i + \Omega$, i.e., from down-conversion originating from the same pump frequency $\omega_p = \omega_s + \omega_i = \omega'_s + \omega'_i$. In [7], $S_{si}^{(2)}(\Omega)$ was proportional to $\delta(\Omega)$ so that the wave functions overlapped only at $\Omega \equiv \omega_s - \omega'_s = 0$, resulting in a coincidence rate independent of the time delay τ .

Since the dependence of this function on τ is known to be in the picosecond range [5,11,12], slower detectors will integrate Eq. (6a) over τ , leading to an integrated fourth-order coherence function

$$G_{si}^{(2)}(\theta_s, \phi_s, \theta_i, \phi_i) = \int d\omega_s \int d\omega_i |\psi(\omega_s, \theta_s, \phi_s, \omega_i, \theta_i, \phi_i)|^2. \quad (7)$$

This function describes the degree of entanglement between the twin photons as a function of their directions. It is proportional to the rate of photon coincidences observed by a pair of detectors with fine angular resolution. The counterpart to Eq. (7) given by Eq. (44) in [7] involves integration over only signal frequencies since, for fixed propagation directions, there is only one idler frequency matching each signal frequency. This is not the case here because of the added tolerance to transverse wave-vector matching.

For coincidence detection through apertures centered at the signal and idler central wave vectors, of respective sizes $\Delta\theta_s \times \Delta\phi_s$ and $\Delta\theta_i \times \Delta\phi_i$, the coincidence rate is proportional to

$$G_{si}^{(2)} = \int_{\Delta\theta_s \times \Delta\phi_s} d\theta_s d\phi_s \int_{\Delta\theta_i \times \Delta\phi_i} d\theta_i d\phi_i \times \int d\omega_s d\omega_i |\psi(\omega_s, \theta_s, \phi_s, \omega_i, \theta_i, \phi_i)|^2. \quad (8)$$

In the case of misalignment of one of the apertures from its central direction, the coincidence rate remains identically as in Eq. (8), with the misalignment accounted for by appropriate change of the limits of integration.

The normalized coincidence rate, which is a measure of the degree of entanglement of the detected photons, is

$$R_{si}^{(2)} \equiv \frac{G_{si}^{(2)}}{\sqrt{I_s I_i}}, \quad (9a)$$

where

$$I_s = \int_{\Delta\theta_s \times \Delta\phi_s} d\theta_s d\phi_s \int d\theta_i d\phi_i \times \int d\omega_s d\omega_i |\psi(\omega_s, \theta_s, \phi_s, \omega_i, \theta_i, \phi_i)|^2 \quad (9b)$$

and I_i is given by a similar expression [7]. Equation (9b) differs from Eq. (8) in that it is integrated over the entire idler space.

B. Gaussian approximations

In order to evaluate the integrals in Eqs. (5a) and (6a), and to obtain explicit expressions for the dependence of the coherence functions on the key parameters of the interacting beams, we make several simplifying assumptions and approximations. The pump spectral distribution is assumed to be a Gaussian function

$$A(\omega) \propto \exp\left[-\frac{(\omega - \omega_p^0)^2}{4\Delta\omega_p^2}\right] \quad (10)$$

and its transverse spatial distribution is also assumed to be a circularly symmetric Gaussian function of x and y , so that its Fourier transform is also Gaussian:

$$F(\mathbf{k}_\perp) \propto \exp\left[-w^2 \frac{k_x^2 + k_y^2}{4}\right]. \quad (11)$$

We also approximate the sinc function in Eq. (4b) by the Gaussian function

$$\text{sinc}\left(\frac{l}{2\pi} \Delta k_z\right) \approx \exp\left[-\frac{(\alpha l \Delta k_z)^2}{4}\right], \quad (12)$$

where $\alpha = 0.430$ is chosen such that the two functions have equal $1/e$ widths.

1. The wave function

Using Eqs. (10)–(12), the twin-state wave function takes the following jointly Gaussian form:

$$\begin{aligned} \psi(\Omega_s, \theta_s, \phi_s, \Omega_i, \theta_i, \phi_i) = N \exp\left[-\frac{1}{4} \left\{ \frac{\phi_s^2}{\sigma_{\phi_s}^2} + \frac{\phi_i^2}{\sigma_{\phi_i}^2} + 2\eta_{\phi_s \phi_i} \phi_s \phi_i \right\}\right] \exp\left[-\frac{1}{4} \left\{ \frac{\Omega_s^2}{\sigma_{\omega_s}^2} + \frac{\Omega_i^2}{\sigma_{\omega_i}^2} + \frac{\theta_s^2}{\sigma_{\theta_s}^2} + \frac{\theta_i^2}{\sigma_{\theta_i}^2} + 2\eta_{\omega_s \omega_i} \Omega_s \Omega_i \right. \right. \\ \left. \left. + 2\eta_{\omega_s \theta_s} \Omega_s \theta_s + 2\eta_{\omega_s \theta_i} \Omega_s \theta_i + 2\eta_{\omega_i \theta_s} \Omega_i \theta_s + 2\eta_{\omega_i \theta_i} \Omega_i \theta_i + 2\eta_{\theta_s \theta_i} \theta_s \theta_i \right\}\right], \quad (13) \end{aligned}$$

where

$$\frac{1}{\sigma_{\phi_s}^2} = \frac{1}{\Delta\phi_{sy}^2}, \quad (14a)$$

$$\eta_{\phi_s \phi_i} = -\frac{1}{\Delta\phi_{sy} \Delta\phi_{iy}}, \quad (14b)$$

$$\frac{1}{\sigma_{\omega_s}^2} = \frac{1}{\Delta\omega_p^2} + \frac{1}{\Delta\omega_{sx}^2} + \frac{1}{\Delta\omega_{sz}^2}, \quad (14c)$$

$$\frac{1}{\sigma_{\theta_s}^2} = \frac{1}{\Delta\theta_{sx}^2} + \frac{1}{\Delta\theta_{sz}^2}, \quad (14d)$$

$$\eta_{\omega_s \omega_i} = \frac{1}{\Delta\omega_p^2} - \frac{1}{\Delta\omega_{sx} \Delta\omega_{ix}} + \frac{1}{\Delta\omega_{sz} \Delta\omega_{iz}}, \quad (14e)$$

$$\eta_{\omega_s \theta_s} = \frac{1}{\Delta\omega_{sx} \Delta\theta_{sx}} - \frac{1}{\Delta\omega_{sz} \Delta\theta_{sz}}, \quad (14f)$$

$$\eta_{\omega_s \theta_i} = -\frac{1}{\Delta\omega_{sx} \Delta\theta_{ix}} - \frac{1}{\Delta\omega_{sz} \Delta\theta_{iz}}, \quad (14g)$$

$$\eta_{\theta_s \theta_i} = -\frac{1}{\Delta\theta_{sx} \Delta\theta_{ix}} + \frac{1}{\Delta\theta_{sz} \Delta\theta_{iz}}, \quad (14h)$$

and the remaining coefficients are given by the interchange of the signal and idler indices. The spectral and angular parameters that appear in Eqs. (14a)–(14h) are given by

$$\Delta\phi_{sy} = \Delta\phi_{iy} = \frac{\lambda_j^0/n_j}{2\pi w \sin\theta_j^0}, \quad (15a)$$

$$\Delta\omega_{jx} = \omega_j^0 \frac{\lambda_j^0/N_j}{2\pi w \sin\theta_j^0}, \quad (15b)$$

$$\Delta\omega_{jz} = \omega_j^0 \frac{\lambda_j^0/(N_j \cos\theta_j^0 - N_p)}{2\pi\alpha l}, \quad (15c)$$

$$\Delta\theta_{jx} = \frac{\lambda_j^0/n_j}{2\pi w \cos\theta_j^0}, \quad (15d)$$

and

$$\Delta\theta_{sz} = \Delta\theta_{iz} = \frac{\lambda_j^0/n_j}{2\pi\alpha l \sin\theta_j^0}, \quad (15e)$$

where $j = s, i$ and the second subscript (x, y , or z) denotes the component of the phase mismatch contributing to the given frequency or angular broadening.

The jointly Gaussian expression for the wave function in Eq. (13) is characterized by coefficients forming a 6×6 matrix that is separable into 2×2 and 4×4 blocks, so that the signal and idler azimuthal angles (ϕ_s and ϕ_i) are uncorrelated with the signal and idler polar angles (θ_s and θ_i) and frequencies (ω_s and ω_i). This factorization follows from the expressions in Eqs. (3a)–(3c) in which only the azimuthal angles determine the wave-vector mismatch in the y direction and do not contribute to the mismatch in the x and z directions. The structure of the 4×4 matrix is indicative of coupling between the signal and idler polar angles and frequencies resulting from their mutual contributions to wave-vector mismatch in the x and the z directions, as indicated by Eqs. (3a) and (3c).

The magnitude of the wave function in Eq. (13) has its maximum value at points in the $(\mathbf{k}_s, \mathbf{k}_i)$ space that are perfectly phase and frequency matched to \mathbf{k}_p^0 and ω_s^0 . These points, in the linear approximation used here, are given by

the line in the (ϕ_s, ϕ_i) plane determined from $\Delta k_y = 0$ in Eq. (3b) (i.e., $\phi_s = \phi_i$) and the line in the $(\Omega_s, \theta_s, \Omega_i, \theta_i)$ space (spectral-polar space) determined from $\Delta k_x = 0$ in Eq. (3a), $\Delta k_z = 0$ in Eq. (3c), and $\Omega_s + \Omega_i = 0$; for the noncollinear and degenerate down-conversion ($\theta_s^0 = \theta_i^0 \neq 0$ and $\omega_s^0 = \omega_i^0$) used here to illustrate the theory and the reported experiment, the spectral-polar line is given by the parametric equations $\theta_i = -\theta_s$, $\Omega_s = -(n_s \omega_s^0 \cot\theta_s^0/N_s)\theta_s$, and $\Omega_i = -\Omega_s$.

2. Second-order coherence function

Using the Gaussian wave function in Eq. (13), the signal second-order coherence function in Eq. (5a) can be cast in the separable form

$$\begin{aligned} G_{ss}^{(1)}(\theta_s, \phi_s, \theta'_s, \phi'_s; \tau) \propto & \exp\left[-\frac{(\phi_s - \phi'_s)^2}{2\phi_s^c}\right] \\ & \times \exp\left[-\frac{(\theta_s - \theta'_s)^2}{2\theta_s^{c^2}}\right] \\ & \times \exp\left[-\frac{\tau^2}{2\tau_s^c}\right] \\ & \times \exp[i\{\omega_s^0 + \xi(\theta_s + \theta'_s)\}\tau]. \end{aligned} \quad (16)$$

The first factor, representing the amplitude coherence of the signal field in the azimuthal direction, is a Gaussian function of width

$$\phi_s^c = 2\sigma_{\phi_s} = \frac{\lambda_s^0/n_s}{\pi w \sin\theta_s^0}, \quad (17)$$

which is the azimuthal signal coherence angle. The second factor in Eq. (16) in which a small term proportional to $\theta_s \theta'_s$ in the exponent has been neglected, represents the amplitude coherence of the signal field in the polar direction and has a width θ_s^c , the polar signal coherence angle, given by

$$\begin{aligned} \frac{1}{\theta_s^c} = & \frac{1}{2\sigma_{\theta_s}^2} - \frac{1}{4} \left(\frac{\eta_{\omega_s \theta_s}^2}{\sigma_{\omega_i}^2 \sigma_{\theta_i}^2} + \frac{\eta_{\omega_i \theta_s}^2}{\sigma_{\omega_s}^2 \sigma_{\theta_i}^2} + \frac{\eta_{\theta_s \theta_i}^2}{\sigma_{\omega_s}^2 \sigma_{\omega_i}^2} - \frac{2\eta_{\omega_s \theta_s} \eta_{\omega_i \theta_s} \eta_{\omega_s \omega_i}}{\sigma_{\theta_i}^2} - \frac{2\eta_{\omega_s \theta_s} \eta_{\theta_s \theta_i} \eta_{\omega_s \theta_i}}{\sigma_{\omega_i}^2} - \frac{2\eta_{\omega_i \theta_s} \eta_{\theta_s \theta_i} \eta_{\omega_i \theta_i}}{\sigma_{\omega_s}^2} \right. \\ & \left. + 2\eta_{\omega_s \theta_s} \eta_{\omega_i \theta_s} \eta_{\omega_s \theta_i} \eta_{\omega_i \theta_i} + 2\eta_{\omega_s \theta_s} \eta_{\theta_s \theta_i} \eta_{\omega_s \omega_i} \eta_{\omega_i \theta_i} + 2\eta_{\omega_i \theta_s} \eta_{\theta_s \theta_i} \eta_{\omega_s \omega_i} \eta_{\omega_s \theta_i} - \eta_{\omega_s \theta_s}^2 \eta_{\omega_i \theta_i}^2 - \eta_{\omega_i \theta_s}^2 \eta_{\omega_s \theta_i}^2 - \eta_{\theta_s \theta_i}^2 \eta_{\omega_s \omega_i}^2 \right) \\ & \times \left(2\eta_{\omega_s \omega_i} \eta_{\omega_s \theta_i} \eta_{\omega_i \theta_i} + \frac{1}{\sigma_{\omega_s}^2 \sigma_{\omega_i}^2 \sigma_{\theta_i}^2} - \frac{\eta_{\omega_s \omega_i}^2}{\sigma_{\theta_i}^2} - \frac{\eta_{\omega_s \theta_i}^2}{\sigma_{\omega_i}^2} - \frac{\eta_{\omega_i \theta_i}^2}{\sigma_{\omega_s}^2} \right)^{-1}. \end{aligned} \quad (18)$$

The third factor is a Gaussian function of τ of width τ_s^c , the signal coherence time, given by

$$\tau_s^c = \frac{1}{\sigma_{\omega_s}^2} + \frac{2\eta_{\omega_s \omega_i} \eta_{\omega_s \theta_i} \eta_{\omega_i \theta_i} \sigma_{\theta_i}^2 \sigma_{\omega_i}^2 - \eta_{\omega_s \omega_i}^2 \sigma_{\omega_i}^2 - \eta_{\omega_s \theta_i}^2 \sigma_{\theta_i}^2}{1 - \eta_{\omega_i \theta_i}^2 \sigma_{\theta_i}^2 \sigma_{\omega_i}^2}. \quad (19)$$

The fourth factor in Eq. (16) indicates a frequency shift

$$\xi(\theta_s + \theta'_s) = -\frac{\overline{\eta}_{\omega_s \theta_s}}{2\tau_s^c}(\theta_s + \theta'_s) \quad (20a)$$

that is a linear function of $\theta_s + \theta'_s$, where

$$\overline{\eta}_{\omega_s \theta_s} = \eta_{\omega_s \theta_s} + \frac{\eta_{\omega_s \omega_i} \eta_{\theta_s \theta_i} \eta_{\omega_i \theta_i} \sigma_{\theta_i}^2 \sigma_{\omega_i}^2 + \eta_{\omega_s \theta_i} \eta_{\omega_i \theta_s} \eta_{\omega_i \theta_i} \sigma_{\theta_i}^2 \sigma_{\omega_i}^2 - \eta_{\omega_s \omega_i} \eta_{\omega_i \theta_s} \sigma_{\omega_i}^2 - \eta_{\omega_s \theta_i} \eta_{\theta_s \theta_i} \sigma_{\theta_i}^2}{1 - \eta_{\omega_i \theta_i}^2 \sigma_{\theta_i}^2 \sigma_{\omega_i}^2}. \quad (20b)$$

As expected from the form of the wave function in Eq. (13), the second-order coherence function factors into a product of a function of azimuthal angles and a function of polar angles and time delay. Thus the signal (and similarly the idler) field is cross-spectrally pure in the azimuthal direction, but not so in the polar direction. The lack of cross-spectral purity of the signal field in the polar direction is exhibited by a signal polar-angle-dependent frequency shift in the fourth factor of Eq. (16). The frequency shift in Eq. (20a) can also be determined directly from the spectral-polar phase and frequency matching line and is independent of

$\Delta\omega_p$, w , and l (it is completely set by phase matching [7]). The signal intensity $I \equiv G_{ss}^{(1)}(\theta_s, \phi_s, \theta_s, \phi_s; 0)$ is independent of direction in this approximation.

The expression for ϕ_s^c in Eq. (17) has the same form as the coherence angle for light emitted from an incoherent source with a circular cross section of diameter $w \sin \theta_s^0$. This might suggest that the second-order coherence properties of spontaneous parametrically down-converted light are equivalent to those of an incoherent source [8]. However, the expressions for θ_s^c and τ_s^c in Eqs. (18) and (19) are very different from those for an incoherent source and incorporate coherent effects imposed by phase- and frequency-matching requirements. The coherence parameters θ_s^c and τ_s^c have a complex dependence on the wave-function coefficients in Eq. (13) resulting from the integration over ω_s, ω_i , and θ_i .

3. Fourth-order coherence function

Using the Gaussian wave function in Eq. (13), the signal-idler fourth-order coherence function in Eq. (6a) can be cast in the separable form

$$G_{si}^{(2)}(\theta_s, \phi_s, \theta_i, \phi_i; \tau) \propto \exp\left[-\frac{(\phi_s - \phi_i)^2}{2\phi_s^e}\right] \times \exp\left[-\frac{(\theta_s + \beta\theta_i)^2}{2\theta_s^e}\right] \exp\left[-\frac{\tau^2}{2\tau^e}\right]. \quad (21)$$

The first factor, representing entanglement in the azimuthal direction, is a Gaussian function of width

$$\phi_s^e = \sigma_{\phi_s} = \frac{\lambda_s^0/n_s}{2\pi w \sin \theta_s^0}, \quad (22)$$

which we call the signal azimuthal entanglement angle. Points for which $\phi_s = \phi_i$ have the highest entanglement, and points for which $|\phi_s - \phi_i|$ exceed ϕ_s^e are weakly entangled. Because of the symmetry of the down-converted luminescence about the pump propagation direction in type-I phase matching, the idler azimuthal entanglement angle ϕ_i^e is equal to its signal counterpart ϕ_s^e (even for nondegenerate down-conversion).

The second factor in Eq. (21), whose exponent is generally a quadratic function of θ_s and θ_i , takes the specific form shown in Eq. (21) for $l \gg w$; it represents entanglement in the polar direction, is a Gaussian function of width θ_s^e , the signal polar entanglement angle, given by

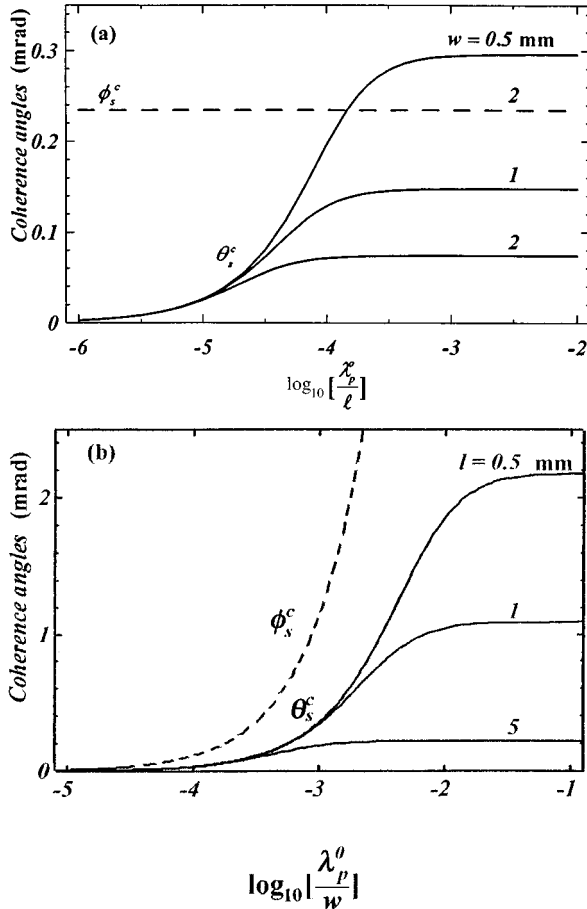


FIG. 2. Dependence of the polar (solid curves) and azimuthal (dashed curves) coherence angle θ_s^c and ϕ_s^c of the signal on (a) the crystal length l for fixed values of the pump-beam waist w and (b) the pump-beam waist w for fixed values of crystal length l . Both coherence angles do not depend on the pump spectral width $\Delta\omega_p$.

$$\frac{1}{\theta_s^e} = \frac{1}{\sigma_{\theta_s}^2} + \frac{2\eta_{\omega_s\omega_i}\eta_{\omega_s\theta_s}\eta_{\omega_i\theta_s}\sigma_{\omega_s}^2\sigma_{\omega_i}^2 - \eta_{\omega_i\theta_s}^2\sigma_{\omega_i}^2 - \eta_{\omega_s\theta_s}^2\sigma_{\omega_s}^2}{1 - \eta_{\omega_s\omega_i}^2\sigma_{\omega_s}^2\sigma_{\omega_i}^2}. \quad (23)$$

The idler polar entanglement angle is given by a similar

expression. This second factor has its peak value when $\theta_s = -\beta\theta_i$, where

$$\beta \equiv \frac{\theta_s^e}{\theta_i^e} = \frac{\lambda_i^0 n_s [N_i \cos(\theta_s^0 + \theta_i^0) - N_s]}{\lambda_s^0 n_i [N_s \cos(\theta_s^0 + \theta_i^0) - N_i]} \quad (24)$$

and $\theta_s^e = \theta_i^e$ only when $\beta = 1$ as in the case of degenerate down-conversion. The third factor is a Gaussian function of τ whose width τ^e , the entanglement time, is given by

$$\tau^e = \frac{1}{4} \left(\frac{1}{\sigma_{\omega_s}^2} + \frac{1}{\sigma_{\omega_i}^2} - 2\eta_{\omega_s\omega_i} \right) = \frac{w^2}{4} \left[\frac{\sin^2 \theta_s^0}{(c/N_s)^2} + \frac{\sin^2 \theta_i^0}{(c/N_i)^2} + \frac{2 \sin \theta_i^0 \sin \theta_s^0}{(c^2/N_i N_s)} \right] + \frac{\alpha^2 l^2}{4} \left[\frac{1}{c^2/(N_s \cos \theta_s^0 - N_p)^2} + \frac{1}{c^2/(N_i \cos \theta_i^0 - N_p)^2} - \frac{2}{c^2/(N_s \cos \theta_s^0 - N_p)(N_i \cos \theta_i^0 - N_p)} \right] \quad (25)$$

The azimuthal dependence of the fourth-order coherence function is expected to factor, as in the case of the second-order coherence function, because of the factorization of the Gaussian wave function itself. In general, Eq. (21) should have a phase factor [as in the case of second-order coherence in Eq. (16) due to the cross term between Ω and the angles θ_s and θ_i]. However, because the fourth-order coherence function is real, the cross term between Ω and the angles cancels out and the polar-temporal part of this coherence function also factors.

The signal azimuthal entanglement angle in Eq. (22) is inversely proportional to the pump waist w and is independent of the pump spectral width $\Delta\omega_p$ and the crystal length l . Also, this angle is related to its corresponding coherence angle by $\phi_s^c = 2\phi_s^e$. This is similar to the situation for incoherent light, in which the Siegert relation is obeyed [9]. In general, the signal and idler polar entanglement angles θ_s^e and θ_i^e , and the signal-idler entanglement time τ^e , depend in a complex manner on all three variables of interest: $\Delta\omega_p$, w , and l . Also, there are no simple relations that we can recognize between these fourth-order coherence parameters and their corresponding second-order coherence parameters. Finally, the fourth-order coherence function in Eq. (21) is constant at $\phi_s - \phi_i = \text{const}$ and $\theta_s + \beta\theta_i = \text{const}$ and the wave function in Eq. (13) is not normalizable.

4. Example

As an example, we consider degenerate noncollinear down-conversion in a lithium iodate (LiIO_3) crystal in the configuration shown in Fig. 1 and determine the dependence of the coherence angles θ_s^c and ϕ_s^c (Fig. 2), the coherence time τ_s^c (Fig. 3), the entanglement angles θ_s^e and ϕ_s^e (Fig. 4), and the entanglement time τ^e (Fig. 5) on $\Delta\omega_p$, w , and l . The following parameters, which are applicable to the experiment reported in Sec. IV, are used: $\lambda_p^0 = 413.1$ nm, $\lambda_s^0 = \lambda_i^0 = 826.2$ nm, $\theta_s^0 = \theta_i^0 = 17.5^\circ$ (internal to the crystal), $n_p = 1.7786$ (extraordinary), $n_s = n_i = 1.8649$ (ordinary), $N_p = 1.9479$, and $N_s = N_i = 1.9095$.

In Fig. 2 we show the dependence of the azimuthal and polar coherence angles ϕ_s^c and θ_s^c , given in Eqs. (17) and (18), respectively, on l [Fig. 2(a)] and w [Fig. 2(b)]. The azimuthal coherence angle depends only on the pump beam

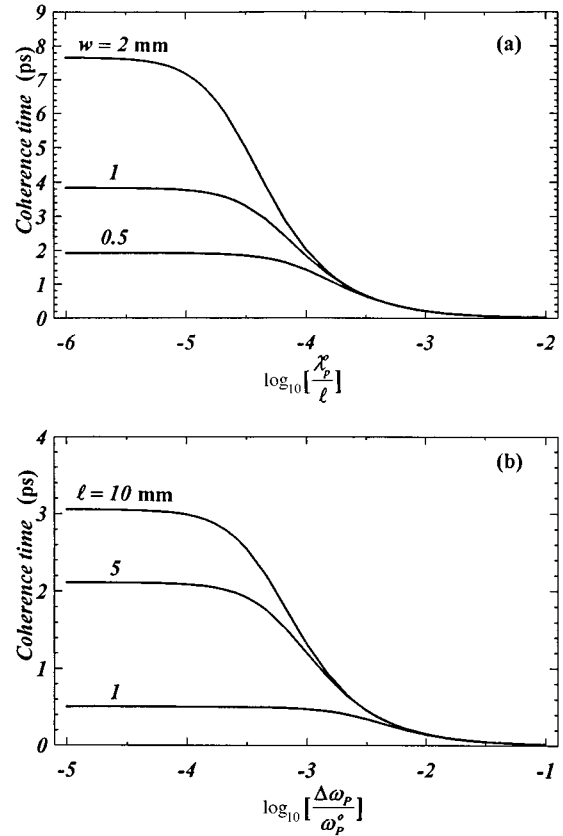


FIG. 3. (a) Dependence of the signal coherence time τ_s^c on the crystal length l for fixed values of the pump-beam waist w and for a pump spectral width fixed at $\Delta\omega_p = 10^{-10}\omega_p^0$. (b) Dependence of τ_s^c on the pump spectral width $\Delta\omega_p$ for fixed values of the crystal length l and fixed beam waist $w = 1$ mm.

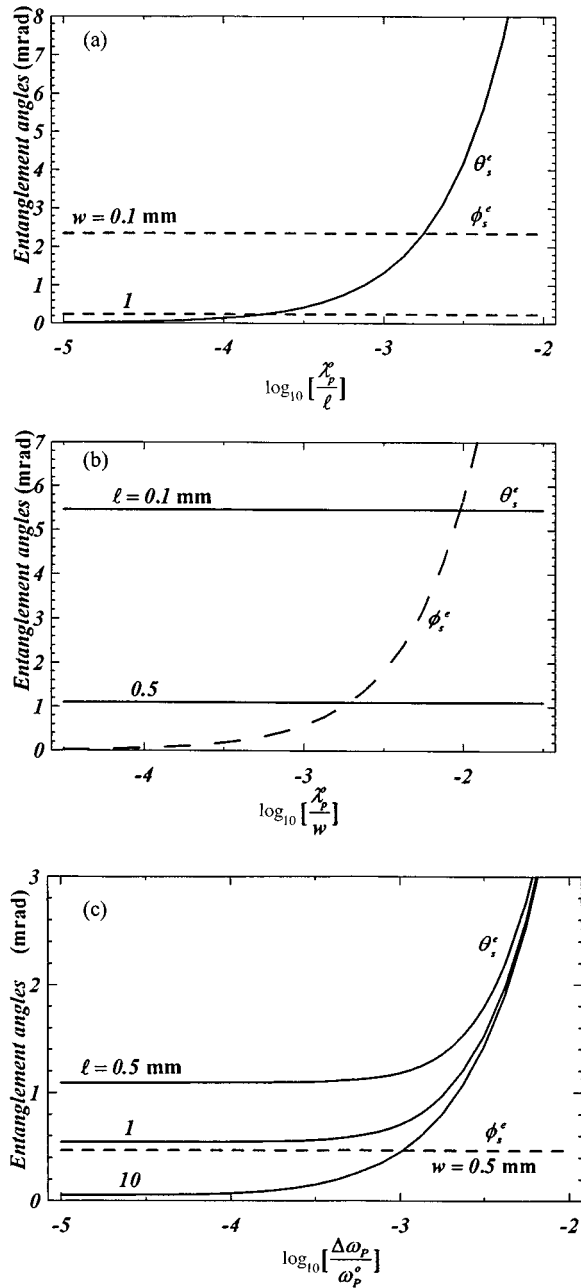


FIG. 4. Dependence of the polar (solid curves) and azimuthal (dashed curves) entanglement angles θ_s^e and ϕ_s^e of the signal on (a) the crystal length l for fixed values of the pump-beam waist w and for $\Delta\omega_p = 10^{-10}\omega_p^0$, (b) the pump-beam waist w for fixed values of crystal length l and for $\Delta\omega_p = 10^{-10}\omega_p^0$, and (c) the pump spectral width $\Delta\omega_p$ for fixed values of the crystal length l and the beam width $w = 0.5 \text{ mm}$.

waist, while the polar coherence angle depends on both the pump beam waist and the crystal length. The polar coherence angle vanishes ($\theta_s^e \rightarrow 0$) as $l \rightarrow \infty$ [$\log_{10}(\lambda_p^0/l) \rightarrow -\infty$] regardless of w . In this limit of exact phase matching in the z direction, there is no overlap between the power spectral densities at two different signal directions θ_s and θ_s^l originating from down-conversion with a fixed idler wave vector [7]. The same is true in the limit $w \rightarrow \infty$. As l decreases (valid for l larger than λ_p^0), θ_s^e increases and saturates to a

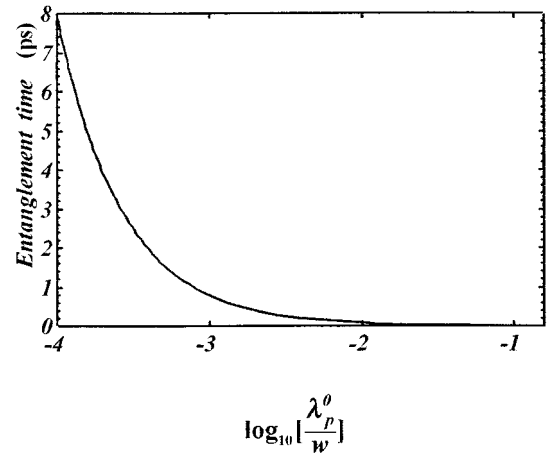


FIG. 5. The entanglement time τ^e in the case of degenerate down-conversion.

fixed value governed by w , i.e., set by the phase-matching requirement in the x direction. A similar result is obtained in the limit of small w . As for the azimuthal coherence angles, it turns out that the polar coherence angle is independent of the pump spectral width $\Delta\omega_p$. This can be explained by the fact that even though a larger $\Delta\omega_p$ corresponds to a larger signal bandwidth, any frequency component of the signal in a fixed direction contributes to the signal cross-power spectrum in other directions extending over the polar coherence angle θ_s^e .

The dependence of the signal coherence time τ_s^c in Eq. (19) on $\Delta\omega_p$, w , and l is shown in Fig. 3. In the limit of large w , large l , or small $\Delta\omega_p$, the coherence time is set by the remaining two parameters. In the opposite limits, the coherence time reduces to zero. As shown in Fig. 3(b), the pump spectral width begins to reduce the coherence time only at relatively large values ($\Delta\omega_p > 10^{-5}\omega_p^0$), so that the often-made assumption of a monochromatic pump is easily achievable (at least in this configuration).

The dependence of the signal entanglement angles ϕ_s^e and θ_s^e on l , w , and $\Delta\omega_p$ is shown in Fig. 4. As expected from Eq. (22), the azimuthal entanglement angle depends only on w . The polar entanglement angle generally depends on all three variables. However, for the degenerate down-conversion case under consideration, it depends on l and $\Delta\omega_p$, but is independent of w . When l is sufficiently large so that exact longitudinal wave-vector matching is required, and for $\theta_i = 0$, fixed ω_p , and different values of ω_i , down conversion occurs only for $\omega_s = \omega_p - \omega_i$ and fixed signal direction. Thus the polar entanglement angle θ_s^e is independent of the beam waist w , as shown in Fig. 4(b). On the other hand, when exact transverse wave vector matching is required and for $\theta_i = 0$, fixed ω_p , and different values of ω_i , down-conversion still occurs only for $\omega_s = \omega_p - \omega_i$ but now the signal direction is a function of ω_i . Thus the polar entanglement angle θ_s^e depends on the crystal length l , as shown in Fig. 4(a). The dependence of θ_s^e on l is similar to the dependence of ϕ_s^e on w ; both θ_s^e and ϕ_s^e are reduced as l or w increase. However, in the limit of small pump spectral width $\Delta\omega_p$, the entanglement angle θ_s^e is governed by the crystal length l and does not approach zero, as shown in Fig. 4(c). The pump spectral width $\Delta\omega_p$ has an effect on the

entanglement angle θ_s^e only at large values ($\Delta\omega_p > 10^{-4}\omega_p^0$).

For degenerate down-conversion, the entanglement time τ^e in Eq. (25) does not depend on the crystal length l ; its dependence on the beam waist w is shown in Fig. 5. In the case of exact longitudinal wave-vector matching, and for $\theta_i=0$, fixed ω_p , and different values of ω_i (i.e., idler photon emitted in the central idler direction), down-conversion occurs only for $\omega_s=\omega_p-\omega_i$ and fixed signal direction $\theta_s=0$ (i.e., the signal photon is emitted in the central signal direction). Thus the width of the fourth-order power spectrum in Eq. (6b), for the given signal-idler directions, is expected to vary in an inverse proportionality to w (even for a monochromatic pump because $\omega_s=\omega_p-\omega_i$ does not fix ω_s and ω_i) and therefore, as shown in Fig. 5, $\tau^e \rightarrow 0$ as $w \rightarrow 0$ and $\tau^e \rightarrow \infty$ as $w \rightarrow \infty$. However, in the case of exact transverse phase matching, and for $\theta_i=0$, fixed ω_p , and different values of ω_i , down-conversion still occurs only for $\omega_s=\omega_p-\omega_i$, but now $\theta_s=\theta_s(\omega_i)$, i.e., the signal photon is emitted in different signal directions depending on the frequency of the idler photon. Therefore, the crystal length l does not contribute to the width of the fourth-order power spectrum in Eq. (6b) and the entanglement time τ^e is independent of l .

Finally, the pump spectral width $\Delta\omega_p$ has no effect on the entanglement time τ^e , in agreement with experimental observations [11].

IV. EXPERIMENT

We have experimentally investigated the predictions of the jointly Gaussian twin state model by measuring coincidence rates of down-converted photons observed through aligned and misaligned apertures of various sizes, as shown in Fig. 6. The 413.1-nm line of a krypton-ion laser was focused to a waist of $w \approx 0.4$ mm to create the pump. A 10-mm-long ($l=10$ mm) lithium iodate crystal was oriented for type-I (ooe) phase matching with the extraordinary pump incident at 90° to the crystal's optic axis. Avalanche photodiodes operated in the photon-counting Geiger mode were used as detectors. They have a diameter of approximately $100 \mu\text{m}$ and were placed at distances of $r_s=738$ mm and $r_i=435$ mm from the center of the crystal. The down-converted light was filtered by RG695 filters placed in front of the detectors to block the pump radiation. The signal and idler directions for degenerate down-conversion were set at maximum coincidence rate when filters centered at 830 nm ($\lambda_s^0=\lambda_i^0=826.2$ nm) and linear polarizers (oriented to let the o rays through) were placed in front of both detectors. The directions obtained were consistent with the computed values of $\theta_s^0=\theta_i^0=17.5^\circ$ (internal to the crystal). The 830-nm filters and polarizers were then removed and one aperture (the signal aperture) was fixed by the detector area, whereas the other aperture (idler aperture) was varied, as shown in Fig. 6. With this setup, we measured the signal-idler coincidence rate, for different idler apertures, as a function of misalignment of the signal aperture in the polar and azimuthal directions.

In Fig. 7 we present the results when the polar and azimuthal signal directions were scanned, in Figs. 7(a) and 7(b), respectively, with both apertures defined by the detector

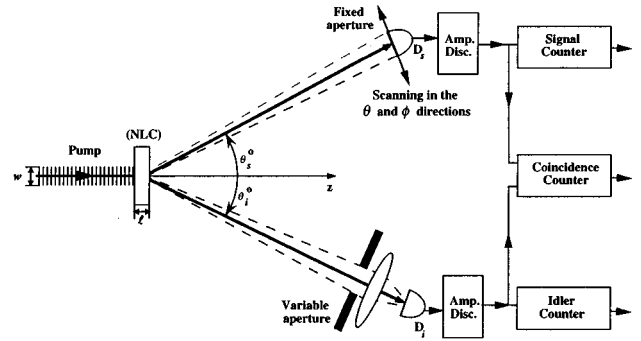


FIG. 6. Experimental setup.

sizes, namely, $\Delta\theta_s=0.063$ mrad, $\Delta\phi_s=0.112$ mrad, $\Delta\theta_i=0.107$ mrad, and $\Delta\phi_i=0.190$ mrad, internal to the crystal. In both cases, the pump power was set at 180 mW and the output pulses from the detectors were counted for 10 s to provide a measure of the rate of photon detection in each of the channels. The sequence of standardized pulses from the two detector were also passed through a 10-ns AND gate and counted for 10 s to provide a measure of the coincidence rate. The dots in the figures represent the raw coincidence data.

In Fig. 8 we present the results when the signal polar direction was scanned, with the signal aperture still set by the detector size and with the idler aperture (determined by a variable aperture and a lens that focused the light onto the idler detector) varied from $\Delta\theta_i=1.069$ mrad and $\Delta\phi_i=1.908$ mrad in Fig. 8(a), to $\Delta\theta_i=2.715$ mrad and $\Delta\phi_i=4.846$ mrad in Fig. 8(b), and to $\Delta\theta_i=3.802$ mrad and $\Delta\phi_i=6.784$ mrad in Fig. 8(c), internal to the crystal. The counting time was set to 10 s and the pump power varied from 75 mW in Fig. 8(a) to 25 mW in Figs. 8(b) and 8(c) to minimize dead-time effects in the idler detector.

To compare these experimental results with the theory, we express the observed coincidence rate in the form

$$R_c = R_{rc} + \eta(R_s R_i)^{1/2} R_{si}^{(2)}, \quad (26)$$

where R_{rc} represents the observed random coincidence rate (determined from completely misaligned apertures), η represents the quantum efficiencies of the signal and idler channels (assumed to be the same for both channels), $R_s = \eta I_s$ and $R_i = \eta I_i$ represent the observed signal and idler single rates, and $R_{si}^{(2)}$ is the normalized coincidence rate in Eq. (9a). This latter quantity is evaluated from the theory by integrating the Gaussian-model expression in Eq. (21) over τ and over the given apertures. The required entanglement angles ϕ_j^e and θ_j^e ($j=s,i$) are evaluated from Eqs. (22) and (23), where the indices of refraction and the group indices of refraction, calculated from Sellmeier formula [17], are $n_p=1.7786$ (extraordinary), $n_s=n_i=1.8649$ (ordinary), $N_p=1.9479$, and $N_s=N_i=1.9095$, as given in the example provided in Sec. III.

This theoretical expression is represented by the solid curves in Figs. 7 and 8. To fit the theory to the experiment we adjusted the values of the entanglement angles by varying l for θ_j^e and varying w for ϕ_j^e ($j=s,i$). We have been able to fit all data sets by choosing $l=7$ mm and $w=0.4$ mm. The

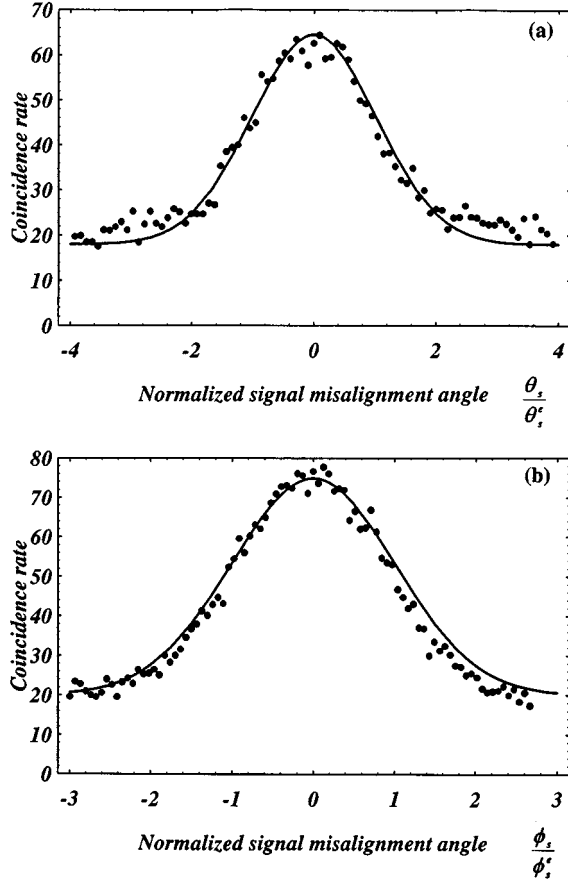


FIG. 7. Experimental data and theoretical curves for the photon coincidence rate (counts per 10 s) as a function of signal aperture misalignment in (a) the θ direction and (b) the ϕ direction. The ratios of the aperture angles to the entanglement angles were $\Delta\theta_s/\theta_s^e=0.35$, $\Delta\phi_s/\phi_s^e=0.19$, $\Delta\theta_i/\theta_i^e=0.59$, and $\Delta\phi_i/\phi_i^e=0.35$; $\eta=0.1$. (a) $R_{rc}=18$, $R_s=17\,930$, and $R_i=39\,036$; (b) $R_{rc}=20$, $R_s=21\,400$, and $R_i=45\,403$.

difference between the actual value of the crystal length, 10 mm, and the value used to achieve the fit, are related to possible walkoff of the signal and idler beams with respect to the pump beam so that an effective crystal length smaller than l determines the phase-matching tolerance [4]. For these values of l and w , the entanglement angles are $\theta_s^e=\theta_i^e=0.181$ mrad and $\phi_s^e=\phi_i^e=0.586$ mrad. The quantum efficiency η required for best fit was 10% in Figs. 7(a) and 7(b), 14% in Figs. 8(a) and 8(b), and 11% in Fig. 8(c), consistent with the 10% efficiency reported in [18], in which a similar experimental apparatus was used. The remaining parameters R_{rc} , R_s , and R_i , required in Eq. (26), are estimated from the data for each plot and are reported in the figure captions.

The effect of aperture mismatch on the normalized coincidence rate $R_{si}^{(2)}$ for perfectly aligned apertures is shown as the solid curve in Fig. 9. Here the signal aperture is fixed at $(\Delta\theta_s \times \Delta\phi_s)/(\theta_s^e \times \phi_s^e)=0.067$, as set by the detector area, and the idler aperture is varied. The dots are calculated by solving for $R_{si}^{(2)}$ using Eq. (26), and substituting from the data, averaged values for the maximum coincidence rate R_c (the coincidence rate for perfect alignment), the random coincidence rate R_{rc} and the singles rates R_s and R_i . The fit is

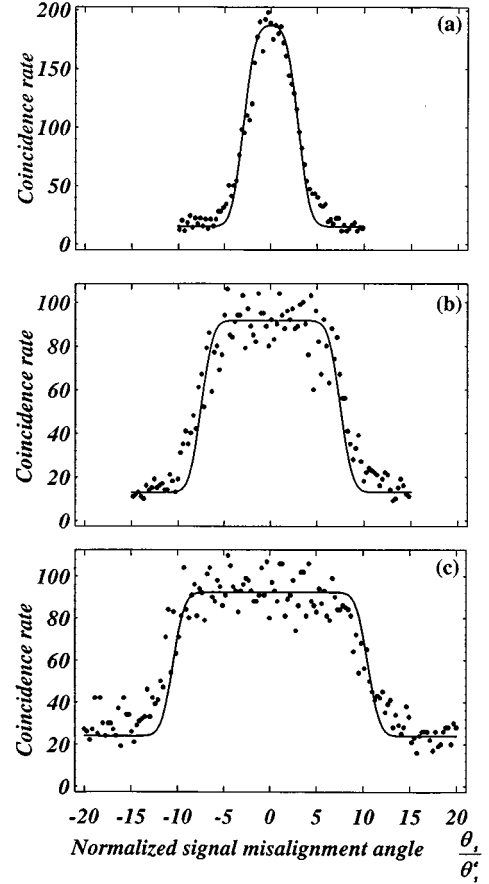


FIG. 8. Experimental data and theoretical curves for the photon coincidence rate (counts per 10 s) as a function of signal aperture misalignment in the θ direction. The normalized signal aperture angles are as in Fig. 6. The remaining parameters are (a) $\Delta\theta_i/\theta_i^e=5.90$, $\Delta\phi_i/\phi_i^e=3.26$, $\eta=0.14$, $R_{rc}=15$, $R_s=9787$, and $R_i=55\,790$; (b) $\Delta\theta_i/\theta_i^e=15.00$, $\Delta\phi_i/\phi_i^e=8.27$, $\eta=0.14$, $R_{rc}=13$, $R_s=4099$, and $R_i=143\,104$; (c) $\Delta\theta_i/\theta_i^e=21.00$, $\Delta\phi_i/\phi_i^e=11.58$, $\eta=0.11$, $R_{rc}=24$, $R_s=6210$, and $R_i=226\,657$.

obtained by setting $\eta=0.13$, which is intermediate between the values used to obtain the best fits in Figs. 7 and 8. The optimal value of $R_{si}^{(2)}$, for the given signal aperture, is 6.1%, which was attainable by choosing $(\Delta\theta_i \times \Delta\phi_i)/(\theta_i^e \times \phi_i^e)=7$. This value of the normalized idler aperture giving the optimal $R_{si}^{(2)}$ is higher than that reported in [7], but the result in [7] is for a one-dimensional model whereas this result is for a two-dimensional model.

V. CONCLUSION

We have developed an approximate Gaussian expression for the wave function of the twin photon beams emitted by the spontaneous parametric down-conversion process, with the effects of pump spectral width, pump beam waist, and crystal length accounted for. This simple model was used to determine the second-order coherence function at pairs of points within the signal (and idler) beams, and the fourth-order coherence function (photon coincidence probability) at

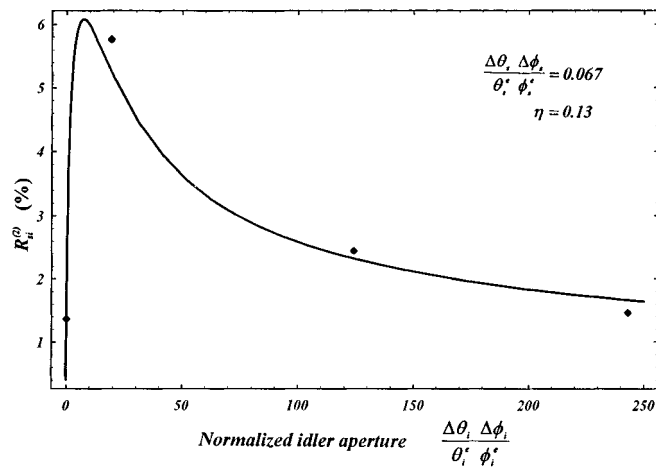


FIG. 9. Experimental data and theoretical fit for the normalized coincidence rate $R_{si}^{(2)}$ as a function of the normalized idler aperture area. The signal and idler apertures are perfectly aligned.

one point within the signal beam and the other within the idler beam.

The magnitude of the second-order coherence function is a product of Gaussian functions of the azimuthal angles, polar angles, and time delay. Its phase is a linear function of time delay, representing a spectral shift that varies with the polar angles. The coherence angles generally decrease as the pump beam width or the crystal length increase. The coherence time increases as the length of the crystal or the beam width increases and also as the pump spectral width is reduced. Although the pump beam possesses complete spatial coherence, the down-converted beam has an elliptically shaped coherence area in this Gaussian model. Even if the pump is perfectly monochromatic, the down-converted light is not.

The photon coincidence rate is also separable as a product of Gaussian functions of the azimuthal angles, polar angles, and time delay, with widths representing the entanglement angles and time. The azimuthal entanglement angle increases with decreasing pump-beam width, but is independent of the crystal length and the pump spectral width. The polar entanglement angle, in contrast, is independent of the pump beam width, but increases with a reduction of the crystal length or an increase of the pump spectral width. The entanglement area is also elliptical, but it does not match the coherence area, so that the Siegert relation [9] is not satisfied. The entanglement time increases with an increase of the pump beam width or with a decrease of the pump spectral width. When the signal and idler photons are collected by apertures of finite area, the photon coincidence rates drop sharply if the aperture areas mismatch the entanglement areas in size or locations. These effects have been demonstrated experimentally.

The Gaussian model of the twin-beam wave function has proven to be very helpful in analytically determining the coherence and photon coincidence properties of parametrically down-converted light. It can also be employed in more general situations such as in interferometers of the following types: Hong-Ou-Mandel [19–21], Michelson [22,23], Mach-Zehnder [6,18,24], and Franson [22,23,25,26]; as well as for light passing through slits as in Young-type experiments [8,14].

ACKNOWLEDGMENTS

This work was supported in part by the Joint Services Electronics Program through the Columbia Radiation Laboratory and by the Office of Naval Research under Grant No. N00014-93-1-0547. We are grateful to H.-B. Fei for verifying many of the results presented here.

-
- [1] D. A. Kleinman, *Phys. Rev.* **174**, 1027 (1968).
 [2] D. C. Burnham and D. L. Weinberg, *Phys. Rev. Lett.* **25**, 84 (1970).
 [3] B. R. Mollow, *Phys. Rev. A* **8**, 2684 (1973).
 [4] D. N. Klyshko, *Photons and Nonlinear Optics* (Gordon and Breach, New York, 1988).
 [5] C. K. Hong and L. Mandel, *Phys. Rev. A* **31**, 2409 (1985).
 [6] R. A. Campos, B. E. A. Saleh, and M. C. Teich, *Phys. Rev. A* **42**, 4127 (1990).
 [7] A. Joobeur, B. E. A. Saleh, and M. C. Teich, *Phys. Rev. A* **50**, 3349 (1994).
 [8] P. H. S. Ribeiro, C. H. Monken, and G. A. Barbosa, *Appl. Opt.* **33**, 352 (1994).
 [9] B. E. A. Saleh, *Photoelectron Statistics* (Springer-Verlag, Berlin, 1978).
 [10] D. N. Klyshko, *Zh. Eksp. Teor. Fiz.* **83**, 1313 (1982) [*Sov. Phys. JETP* **56**, 753 (1982)].
 [11] S. Friberg, C. K. Hong, and L. Mandel, *Phys. Rev. Lett.* **54**, 2011 (1985).
 [12] I. Abram, R. J. Raj, J. L. Oudar, and G. Dolique, *Phys. Rev. Lett.* **57**, 2516 (1986).
 [13] T. P. Grayson and G. A. Barbosa, *Phys. Rev. A* **49**, 2948 (1994).
 [14] P. H. S. Ribeiro, S. Pádua, J. C. Machado da Silva, and G. A. Barbosa, *Phys. Rev. A* **49**, 4176 (1994).
 [15] Z. Y. Ou, L. J. Wang, and L. Mandel, *Phys. Rev. A* **40**, 1428 (1989).
 [16] R. J. Glauber, *Phys. Rev.* **130**, 2529 (1963).
 [17] *Handbook of Laser Science and Technology*, edited by M. J. Weber (CRC, Boca Raton, FL, 1986), Vol. III, p. 108.
 [18] T. S. Larchuk, R. A. Campos, J. G. Rarity, P. R. Tapster, E. Jakeman, B. E. A. Saleh, and M. C. Teich, *Phys. Rev. Lett.* **70**, 1603 (1993).
 [19] C. K. Hong, Z. Y. Ou, and L. Mandel, *Phys. Rev. Lett.* **59**, 2044 (1987).
 [20] Z. Y. Ou and L. Mandel, *Phys. Rev. Lett.* **61**, 54 (1988).
 [21] J. G. Rarity and P. R. Tapster, *J. Opt. Soc. Am. B* **6**, 1221 (1989).
 [22] J. Brendel, E. Mohler, and W. Martienssen, *Phys. Rev. Lett.* **66**, 1142 (1991).

- [23] J. Brendel, E. Mohler, and W. Martienssen, *Europhys. Lett.* **20**, 575 (1992).
- [24] J. G. Rarity, P. R. Tapster, E. Jakeman, T. S. Larchuk, R. A. Campos, M. C. Teich, and B. E. A. Saleh, *Phys. Rev. Lett.* **65**, 1348 (1990).
- [25] J. D. Franson, *Phys. Rev. Lett.* **62**, 2205 (1990).
- [26] J. G. Rarity, J. Burnett, P. R. Tapster, and R. Paschotta, *Europhys. Lett.* **22**, 95 (1993).